41st Annual International Conference of the IEEE Engineering in Medicine and Biology Society

July 23-27 2019

Messe Berlin
Berlin, Germany

Conference Chair

Thomas Penzel, Charité University Medicine Berlin, Germany

Conference Co-Chairs

Thomas Lenarz, Medical University of Hannover (MHH), Germany

Mohamad Sawan, Westlake University Hangzhou, China

Program Chair

Olaf Dössel, Karlsruhe Institute of Technology, Germany

Program Co-Chairs

Luca Mainardi, Politecnico di Milano, Italy
Konstantina S. Nikita, National Technical University of Athens, Greece
James Weiland, University of Michigan Ann Arbor, United States

IEEE Advancing Technology for Humanity

EMB

Indexed in PubMed® and MEDLINE®, Products of the United States National Library of Medicine

PubMed MEDLINE U.S. National Library of Medicine

Table of Contents

18:00-19:30 FrPOS-08.8
A Novel Hand-Held based Diffuse Optical Tomography Device for Breast Tumor Detection
Guo, Jia-Jiun *(National Chiao Tung Univ.)*; Wu, Wen-Jun *(National Chiao Tung Univ.)*; Fang, Wai-Chi* *(National Chiao Tung Univ.)*

18:00-19:30 FrPOS-08.9
MBLL with Weighted Partial Path Length for Multi-Distance Probe Configuration of fNIRS
Song, Xizi *(Tianjin Univ.)*; Chen, Xinrui* *(Tianjin Univ.)*; Wang, Zhongpeng *(Tianjin Univ.)*; An, Xingwei *(Tianjin Univ.)*; Ming, Dong *(Tianjin Univ.)*

18:00-19:30 FrPOS-08.10
Dual Layered Models of Light Scattering in the Near Infrared A: Optical Measurements and Simulation
Almajidy, Rand Kasim *(Univ. Medical Center, Freiburg Dept. of Neurosurgery)*; Rackebrandt, Klaas *(Unity AG, Hamburg)*; Gehring, Hartmut *(Dept. of Anaesthesiology, Univ. of Luebeck, Luebeck)*; Hofmann, Ulrich G.* *(Univ. of Freiburg)*

18:00-19:30 FrPOS-08.11
Dual Layered Models of Light Scattering in the Near Infrared B: Experimental Results with a Phantom
Almajidy, Rand Kasim *(Univ. Medical Center, Freiburg Dept. of Neurosurgery)*; Rackebrandt, Klaas *(Unity AG, Hamburg)*; Gehring, Hartmut *(Dept. of Anaesthesiology, Univ. of Luebeck, Luebeck)*; Hofmann, Ulrich G.* *(Univ. of Freiburg)*

18:00-19:30 FrPOS-08.12
Superficial Fluctuations in Functional Near-Infrared Spectroscopy
Zhang, Fan* *(Univ. of Oklahoma)*; Cheong, Daniel *(Univ. of Oklahoma)*; Chen, Yuxuan *(Univ. of Oklahoma)*; Khan, Ali Fahim *(Univ. of Oklahoma)*; Ding, Lei *(Univ. of Oklahoma)*; Yuan, Han *(Univ. of Oklahoma)*

18:00-19:30 FrPOS-08.13
Automatic Identification of Mixed Retinal Cells in Time-Lapse Fluorescent Microscopy Images using High-Dimensional DBSCAN
Appapogu, Divya Spoorthy *(IIT Hyderabad)*; Manne, Shanmukh Reddy* *(Indian Institute of Technology Hyderabad)*; Dhyani, Vaibhav *(Indian Institute of Technology Hyderabad,)*; Swain, Sarpras *(Indian Institute of Technology, Hyderabad)*; Shahulhameed, Shahna *(L V Prasad Eye Institute Hyderabad)*; Mishra, Siddhartha *(IIT Hyderabad)*; Kaur, Inderjeet *(L V Prasad Eye Institute Hyderabad)*; Giri, Lopamudra *(Indian Institute of Technology Hyderabad)*; Jana, Soumya *(Indian Institute of Technology Hyderabad)*

18:00-19:30 FrPOS-08.14
In Silico Modelling of Blood Vessel Segmentations for Estimation of Discretization Error in Spatial Measurement and its Impact on Quantitative Fluorescence Angiography
Naber, Ady* *(Karlsruhe Institute of Technology)*; Berwanger, Daniel *(Karlsruhe Institute of Technology)*; Nahm, Werner *(Karlsruhe Institute of Technology)*

FrPOS-09: 18:00-19:30 Hall B
Other and Novel Imaging Applications – Poster (Poster Session)

18:00-19:30 FrPOS-09.1
A Method for Multi-Day Tracking of Gastrointestinal Smooth Muscle Contractile Patterns in Organotypic Culture
Du, Peng* *(The Univ. of Auckland)*; Mazzone, Amelia *(Mayo Clinic)*; Calder, Stefan *(Auckland Bioengineering Institute, Univ. of Auckland)*; Qian, Anna *(The Univ. of Auckland)*; Gibbons, Simon J *(Mayo Clinic College of Medicine)*; Farrugia, Gianrico *(Mayo Clinic College of Medicine)*; Beyder, Arthur *(Mayo Clinic)*

18:00-19:30 FrPOS-09.2
Exploring the Supra Linear Relationship between PetCO2 and fMRI Signal Change with ICA
Callara, Alejandro Luis* *(Dipartimento di Ingegneria dell'Informazione, Univ. of Pisa)*; Morelli, Maria Sole *(Scuola Superiore Sant'Anna (Pisa))*; Cauzzo, Simone *(Scuola Superiore Sant'Anna, Institute of Life Science)*; Giannoni, Alberto *(Fondazione Gabriele Monasterio, Pisa)*; Hartwig, Valentina *(Univ. of Pisa)*; Montanaro, Domenico *(Fondazione Toscana "G. Monasterio", National Research Council, P)*; Landini, Luigi *(Univ. of Pisa)*; Passino, Claudio *(Fondazione Gabriele Monasterio, Pisa)*; Emdin, Michele *(Fondazione Gabriele Monasterio, Pisa)*; Vanello, Nicola *(Univ. of Pisa)*

18:00-19:30 FrPOS-09.3
3D Ultrasound Spine Image Selection using Convolution Learning-to-Rank Algorithm
Lyu, Juan *(Harbin Engineering Univ.)*; Ling, Sai Ho, Steve* *(Univ. of Technology Sydney)*; Banerjee, Sunetra *(Univ. of Technology Sydney)*; Zheng, Jenny *(Imperial College London)*; Lai, Ka Lee *(The Hong Kong Polytechnic Univ.)*; Yang, De *(The Hong Kong Polytechnic Univ.)*; Zheng, Yong-Ping *(The Hong Kong Polytechnic Univ.)*; Su, Steven Weidong *(Univ. of Technology, Sydney)*

18:00-19:30 FrPOS-09.4
A Novel Scanning Algorithm for MEG/EEG Imaging using Covariance Partitioning and Noise Learning
Cai, Chang *(University of California, San Francisco)*; Sekihara, Kensuke *(Tokyo Metropolitan University)*; Nagarajan, Srikantan S.* *(University of California, San Francisco)*

18:00-19:30 FrPOS-09.5
Towards Automatic Artifact Rejection in Resting-State MEG Recordings: Evaluating the Performance of the SOUND Algorithm
Rodríguez-González, Víctor *(Biomedical Engineering Group, University of Valladolid)*; Poza, Jesus* *(University of Valladolid)*; Núñez, Pablo *(University of Valladolid)*; Gomez, Carlos *(University of Valladolid)*; Garcia, Maria *(University of Valladolid)*; Shigihara, Yoshihito *(Precision Medicine Center, Hokuto Hospital)*; Hoshi, Hideyuki *(Precision Medicine Center, Hokuto Hospital)*; Santamaría, Eduardo *(University of Valladolid)*; Hornero, Roberto *(University of Valladolid)*

18:00-19:30 FrPOS-09.6
Bidimensional Fuzzy Entropy: Principle Analysis and Biomedical Applications
Hilal, Mirvana* *(University of Angers)*; Humeau-Heurtier, Anne *(University of Angers)*

18:00-19:30 FrPOS-09.7
Statistical Shape-Kinematics Models of the Skeletal Joints: Application to the Shoulder Complex
Foueface, Jean-Rassaire* *(Univ. of Cape Town)*; Alemneh, Tewodros *(Univ. of Cape Town)*; Borotikar, Bhushan *(Univ. of Western Brittany)*; Burdin, Valerie *(IMT Atlantique/Institut Mines Telecom)*; Douglas, Tania S *(Univ. of Cape Town)*; Mutsvangwa, Tinashe Ernest Muzvidzwa *(Univ. of Cape Town)*

18:00-19:30 FrPOS-09.8
Three-Dimensional Distorted Born Iterative Method Enhanced by Breast Boundary Extraction for Microwave Mammography
Noritake, Kazuki *(University of Electro-Communications)*; Kidera, Shouhei* *(University of Electro-Communications)*

Towards Automatic Artifact Rejection in Resting-State MEG Recordings: Evaluating the Performance of the SOUND Algorithm

Víctor Rodríguez-González, Jesús Poza, *IEEE Senior Member*, Pablo Núñez, Carlos Gómez, *IEEE Senior Member*, María García, *IEEE Senior Member*, Yoshihito Shigihara, Hideyuki Hoshi, Eduardo Santamaría-Vázquez, Roberto Hornero, *IEEE Senior Member*

***Abstract*— In this study, a new automated noise rejection algorithm, the SOurce-estimate-Utilizing Noise-Discarding algorithm (SOUND), was evaluated on magnetoencephalographic (MEG) resting-state signals in order to select its optimal configuration parameters. Different values of the epoch length and the regularization parameter λ_0 were assessed in three scenarios with ascending noise levels. Results show that it is possible to remarkably improve the Signal-to-Noise Ratio, without overly altering the signal of interest. An optimal λ_0 value of 0.1 was obtained. However, the epoch length should be adapted to the specific problem. In conclusion, our results suggest that the SOUND algorithm is an appropriate and useful tool to be applied in a preprocessing pipeline for MEG resting-state signals.**

I. INTRODUCTION

Magnetoencephalography (MEG) is an electrophysiological brain imaging method, which records magnetic signals generated by neurons at the scalp level. MEG has a high economic cost, but provides low invasivity and high temporal and spatial resolution [1]. This offers advantages over other brain imaging techniques like electroencephalography, functional magnetic resonance imaging and positron emission tomography, which suffer from low spatial resolution, low temporal resolution and high invasivity level, respectively [1].

MEG can be used in clinical environments to detect cerebral injuries or tumors, to study cognitive processes in fetuses and newborns, or to localize foci on epileptic patients, among others [2]. MEG is also widely used in research scenarios related to many neurodegenerative diseases, such as Alzheimer [3], schizophrenia, or bipolar disorder [4].

This research was supported by 'European Commission' and 'European Regional Development Fund' (FEDER) under project 'Análisis y correlación entre el genoma completo y la actividad cerebral para la ayuda en el diagnóstico de la enfermedad de Alzheimer' ('Cooperation Programme Interreg V-A Spain-Portugal, POCTEP 2014-2020'), and by 'Ministerio de Ciencia, Innovación y Universidades' and FEDER under project DPI2017-84280-R.

V. Rodríguez-González, P. Núñez, J. Poza, C. Gómez, M. García, E. Santamaría, and R. Hornero are with the Biomedical Engineering Group, University of Valladolid, Valladolid, Spain (corresponding author's e-mail: victor.rodriguez@gib.uva.es).

Y. Shigihara and H. Hideyuki are with Precision Medicine Centre, Hokuto Hospital, Obihiro, Japan.

V. Rodríguez-González was in receipt of a PIF-UVa grant from the University of Valladolid. P. Núñez was in receipt of a predoctoral scholarship 'Ayuda para contratos predoctorales para la Formación de Profesorado Universitario (FPU)' grant from the 'Ministerio de Educación, Cultura y Deporte' (FPU17/00850).

There are two main types of MEG recordings: (i) evoked responses, which measure the brain response to a certain motor, sensory or cognitive event; and (ii) resting-state, where the brain activity is recorded when an explicit task is not being performed [1].

In both cases, in order to perform an effective analysis, a preprocessing of the MEG signals has to be applied. This process should reduce the presence of noise from different sources in the cortical signals. For this purpose, different methods can be applied, like filtering, umbralization, independent component analysis or source space projection [5], [6], [7]. However, some of these procedures are not purely objective and suffer from a great dependence on the criteria of the professional who performs the analyses [6], [7].

In order to develop a fully automated preprocessing algorithm, a quantitative way of rejecting noise is required. This would allow an objective and professional-independent noise rejection process [8], [9]. This issue has been addressed by many research groups, which have developed different automated processes for noise rejection [8], [9], [10], [11]. In this paper, we have assessed the SOurce-estimate-Utilizing Noise-Discarding (SOUND) algorithm due to its outperformance over other preprocessing techniques and its ease of use [8]. The SOUND algorithm provides a fully automated artifact rejection method. It uses the source-level signals to cross-validate the information between sensors. The algorithm has been previously tested with evoked responses [8], but not with resting-state signals. Hence, this paper focused on evaluating the algorithm with the latter. Moreover, we wanted to determine the optimal parameter values to establish a fully automated pipeline of applying SOUND on MEG resting-state recordings.

II. SUBJECTS AND MEG RECORDINGS

The sample consisted of 3 subjects: 2 male (aged 83 and 85 years) and 1 female (aged 94 years). The corresponding MEG recordings were inspected by a specialist and classified in three scenarios with ascending noise levels (low, medium, and high) showing different types of artifacts (cardiac, ocular, movement, etc.).

The Ethical Committee of the Hokuto Hospital (Obihiro, Japan) approved the study according to the Code of Ethics of the World Medical Association (Declaration of Helsinki).

MEG recordings were obtained using a 160-channel axial gradiometer MEG system (Yokogawa-KIT, Yokogawa Elec-

978-1-5386-1311-5/19/$31.00 ©2019 Crown

tric) at the Hokuto Hospital, Obihiro, Japan. MEG activity was recorded at a sampling rate of 1000 Hz. Subjects were asked to keep their eyes closed and to remain still and awake during MEG acquisition. To prevent somnolence, MEG activity was monitored in real time. Eighty seconds of resting-state MEG activity were selected for each subject.

III. METHODS

A. The SOUND Algorithm

The SOUND algorithm is a Wiener estimator that minimizes the mean-squared error in the estimated clean signal [8]. SOUND uses anatomical information of the head from a forward model to make a cross-validation of the information in different sensors. Thereby, noise and artifacts can be identified and removed from the signal of interest [8].

The signal measured by sensor *S* at *T* time points, $\mathbf{Y}$, can be written as [8]:

$$\mathbf{Y} = \overline{\mathbf{Y}} + \mathbf{N} = \mathbf{L}\mathbf{J} + \mathbf{N}, \tag{1}$$

being $\mathbf{Y}$ the measured data, $\overline{\mathbf{Y}}$ the noiseless data, $\mathbf{N}$ the noise, $\mathbf{L}$ the leadfield matrix, and $\mathbf{J}$ the clean source-level data.

To estimate $\overline{\mathbf{Y}}$ from $\mathbf{Y}$, a clean estimation of the noiseless source-level signal, $\mathbf{J}$, is needed. For this task, the noise covariance matrix, $\mathbf{\Sigma}$, is needed. If we consider the noise to be uncorrelated across sensors, $\mathbf{\Sigma}$ becomes a diagonal matrix $\mathbf{\Sigma}$=diag(σ_1,σ_2,...,σ_s) [8]. Thus, it can be calculated by estimating the noise signal, σ_s, in each sensor as [8]:

$$\sigma_s = \sqrt{\frac{\sum_{t=1}^{T} y_{s,t} - \mathbf{l}_s \bar{\mathbf{j}}_{.,t}}{T}}, \tag{2}$$

where $y_{s,t}$ is the signal measured by the sensor *s* in the instant *t*, $\mathbf{l}_s$ is the row *s* of the leadfield matrix, and $\bar{\mathbf{j}}_{.,t}$ is the source-level signal in the time instant *t*.

SOUND estimates the noise iteratively [8]:

1) Re-reference the data to a sensor with a low noise level, producing an initial $\mathbf{\Sigma}$ estimate.
2) Estimate σ_s in all sensors and update the $\mathbf{\Sigma}$ value.
3) Repeat step 2 until the convergence of $\mathbf{\Sigma}$.

With the final $\mathbf{\Sigma}$ estimation, the clean source-level signal estimation $\widehat{J}$, and thus the estimated denoised sensor-level signal $\widehat{Y}$ can be reconstructed [8].

In short, SOUND uses the multidimensional nature of the data and anatomical information to estimate the reliability of the sensors, cleaning the data accordingly [8].

B. Configuration of SOUND parameters

To apply SOUND properly, a leadfield matrix is needed for the transformation between scalp and source level. The computations of the leadfield matrices was accomplished using the MEAW Toolboox, developed by Yoshihito Shigihara and Hideyuki Hoshi [12]. Additionally, to construct the leadfield matrix, a MNI152 template was used.

The number of iterations has to be large enough to allow the convergence of the algorithm [8]. Several tests were performed, showing that 20 iterations are enough to converge in all the scenarios.

C. Evaluation of the algorithm performance

1) Visual signal inspection: In a first step, MEG signals were visually inspected to identify whether an artifact had been removed.

2) Signal-to-Noise Ratio and Overcorrection Tradeoff: In order to make a quantitative evaluation of the performance of SOUND, two parameters had to be optimized: the signal-to-noise ratio variation between trials (Δ*SNR*) and the overcorrection (*OC*). Δ*SNR* measures the quantity of noise rejected from the signal, whereas *OC* shows the amount of information (signal of interest) that has been removed along with the noise. A tradeoff between both parameters should be found. Δ*SNR* is calculated as follows [8]:

$$\Delta SNR = \left\langle \frac{\frac{\|\hat{\mathbf{y}}_s^1\|}{\|\hat{\mathbf{y}}_s\|} - \frac{\|\mathbf{y}_s^1\|}{\|\mathbf{y}_s\|}}{\frac{\|\mathbf{y}_s^1\|}{\|\mathbf{y}_s\|}} \times 100 \right\rangle, \tag{3}$$

where $\mathbf{y}_s$ and $\hat{\mathbf{y}}_s$ are the original and the denoised signals in sensor s, respectively, $\|\cdot\|$ refers to the L_2 norm, and $\langle\cdot\rangle$ is the mean value [8]. The superscript ^{1} indicates that the signals have been filtered around the individual alpha frequency (IAF) $\pm$2.5 Hz (Hamming window, order 3000). The IAF was calculated as the median frequency of the power spectral density in the range of 4 to 15 Hz [13], [14]. The IAF$\pm$2.5 Hz band has been considered since it encloses the dominant activity during resting-state recordings [13], [14].

OC was calculated as the absolute value of the correlation coefficient between the noiseless signal and the estimated noise [8]:

$$OC = \left\langle \frac{\left|\hat{\mathbf{y}}_s(\mathbf{y}_s - \hat{\mathbf{y}}_s)^T\right|}{\|\hat{\mathbf{y}}_\mathbf{s}\|_2 \, \|\mathbf{y}_\mathbf{s} - \hat{\mathbf{y}}_\mathbf{s}\|_2} \right\rangle. \tag{4}$$

Additionally, λ_0 is a regularization parameter that controls the balance between preserving the signal of interest and removing noise. More details about λ_0 could be found in [8]. In order to objectively choose λ_0, a trade-off parameter, κ, was defined. κ has to be maximized to offer the optimal compromise between maximizing the Δ*SNR* and minimizing the *OC*. The algorithm tradeoff was then calculated as follows:

$$\kappa = \frac{\Delta SNR^n}{OC^n}, \tag{5}$$

where the superscript ^{n} means that the values have been z-normalized.

IV. RESULTS AND DISCUSSION

A. Optimizing the epoch length

Lower values of the epoch length yield a greater Δ*SNR* and slightly lower *OC*, as shown in Fig. 1. However, they also cause new artifacts due to edge effects. The number of emerged artifacts is related to the epoch length, which determines the number of epochs. Likewise, the artifact amplitude depends on the local power of each epoch. Consequently,

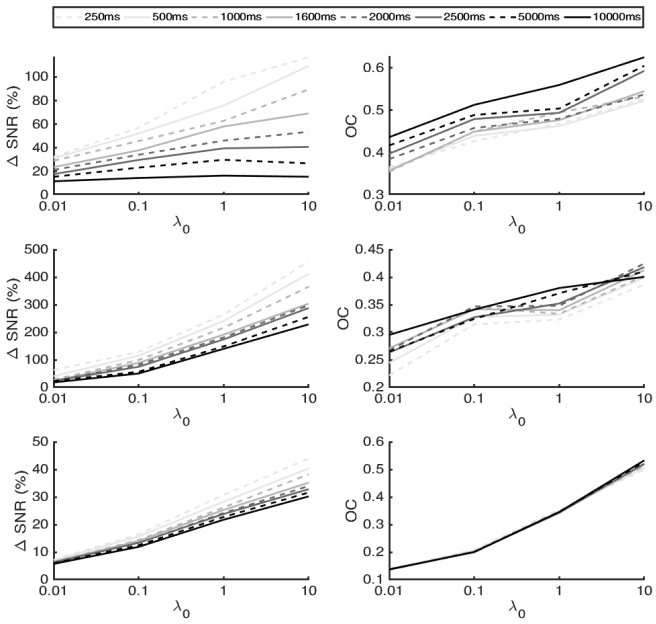

Fig. 1. SNR and OC values as a function of λ_0 parameter and epoch length: the first row shows the high noise scenario, the second row the medium noise scenario, and the last row the low noise scenario.

a compromise when choosing an optimal epoch length is needed. Using smaller epoch lengths increase the algorithm performance because it improves the assumption of noise stationarity. Nevertheless, the artifacts related to edge effects are not reflected in Fig. 1, due to the ΔSNR estimation used [8]. Fig 2 shows an example of the aforementioned artifact caused by the edge effects. Additionally, these artifacts would not be removed because they appear after applying SOUND.

In conclusion, the epoch length should be adapted to the particular characteristics of the problem at hand. When using SOUND as a first stage in an automated pipeline, the selection of the epoch length should take into account the remaining stages of the method and the effect of the aforementioned artifacts on the signal.

B. Optimizing λ_0

The dependence of the ΔSNR and OC values as a function of λ_0 and epoch length can be seen in Fig. 1. Both parameters increase their values with λ_0 for all the assessed scenarios. The objective was to obtain a high ΔSNR, while keeping the OC low; therefore a compromise between these two variables when choosing the λ_0 parameter has to be found. An overly large λ_0 value would lead to a large quantity of the signal of interest to be removed. On the other hand, if the value of λ_0 is not high enough, the artifacts would not be removed at all.

Fig. 3 shows the κ values as a function of λ_0. The largest values of κ were obtained for λ_0=0.1. This value yielded the best compromise between maximizing the ΔSNR and minimizing the OC. These results agree with the findings in the original SOUND paper [8].

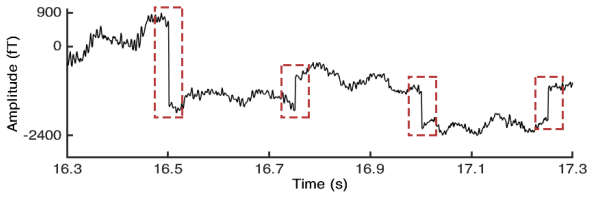

Fig. 2. Artifact caused by edge effects after applying SOUND with 250ms epoch length. Red boxes marks the aforementioned artifacts

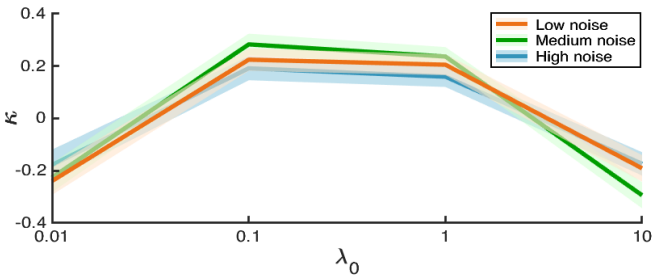

Fig. 3. Algorithm tradeoff κ as a function of λ_0 parameter. The figure shows the mean and standard error of the algorithm tradeoff for the high (blue), medium (green) and low (orange) noise level scenarios.

C. Assessing the performance of the algorithm

Table I shows ΔSNR and OC values for the three studied scenarios. ΔSNR values have been split between the channels where the signal-to-noise ratio increased or decreased.

These values show that, quantitatively, SOUND increases the signal-to-noise ratio from the resting-state MEG signals, while keeping the OC low. These results are in agreement with those obtained by Mutanen *et al.* [8], which support the use of SOUND with MEG resting-state recordings.

In Fig. 4 the noise rejection performed by SOUND is illustrated. This figure shows different types of artifacts, and how the SOUND algorithm can detect and remove them. Moreover, Fig 4 depicts the topography of the log-transformed power in the IAF±2.5 Hz band, before and after applying SOUND. After the application of the SOUND algorithm, alpha activity in posterior brain regions appears, which is typically observed in resting-state studies [13], [14].

TABLE I

ΔSNR AND OC VALUES OBTAINED FOR THE DIFFERENT NOISE LEVEL SCENARIOS UNDER STUDY

	SCENARIOS		
	High noise	**Medium noise**	**Low noise**
	Value	Value	Value
ΔSNR (%)	36.9 (160)	87.0 (160)	14.0 (160)
$\Delta SNR\uparrow$ (%)	51.5 (152)	176.6 (149)	25.8 (137)
$\Delta SNR\downarrow$ (%)	-3.1 (8)	-6.7 (11)	-3.9 (23)
OC	0.46 (160)	0.33 (160)	0.20 (160)

ΔSNR, $\Delta SNR\uparrow$, and ΔSNR$\downarrow$ represent respectively all, improved, and worsened channels after applying SOUND. The values in brackets show the number of channels in each category

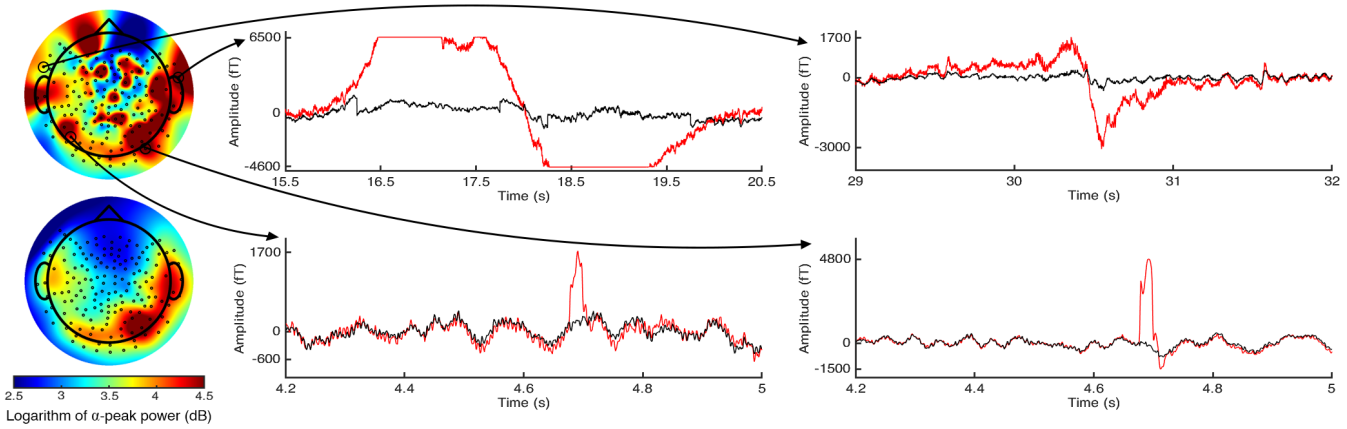

Fig. 4. Left column shows the topography of the log-transformed power for the band centered on the individual alpha peak (IAF±2.5 Hz), before (upper row) and after (lower row) applying SOUND. Central and right columns show different types of noise artifacts that the algorithm has been able to remove. The red curves show the noisy MEG signals, while the black curves show the reconstructed signals.

D. Limitations and future lines

Several limitations of this study should be pointed out. Firstly, the SOUND algorithm was evaluated in three MEG recordings with different noise levels. Future studies should include a larger database. No synthetic signals were used altough they could provide higher accuracy when measuring the performance of SOUND. However, generating synthetic real-wise signals is not straightforward and requires further research. The high computational cost associated with the SOUND algorithm has prevented us from studying a large range of λ_0 and epoch length values. Future studies would be aimed at analyzing additional values of these parameters.

V. CONCLUSIONS

The SOUND algorithm has been assessed on MEG resting-state signals. Our results suggest that the SOUND algorithm is an appropriate method to be included in a fully automated preprocessing protocol of MEG resting-state signals.

Our results also indicate that a $\lambda_0 = 0.1$ value offers an optimal balance between maximizing the *SNR* in the reconstructed signal, while keeping the overcorrection as low as possible. On the other hand, it has not been possible to establish an optimal value of epoch length, suggesting that it should be adapted to each specific problem.

ACKNOWLEDGMENT

Authors would like to thank to T. Mutanen for his support with our queries regarding the SOUND algorithm.

REFERENCES

[1] C. Babiloni, V. Pizzella, C. D. Gratta, A. Ferretti, and G. L. Romani, "Fundamentals of electroencephalography, magnetoencephalography, and functional magnetic resonance imaging," *Int. Rev. Neurobiol.*, vol. 86, no. 9, pp. 67–80, 2009.

[2] X. De Tiège, D. Lundqvist, S. Beniczky, S. Seri, and R. Paetau, "Current clinical magnetoencephalography practice across Europe: Are we closer to use MEG as an established clinical tool?" *Seizure*, vol. 50, no. 1, pp. 53–59, 2017.

[3] M. Engels, W. van der Flier, C. Stam, A. Hillebrand, P. Scheltens, and E. van Straaten, "Alzheimer's disease: The state of the art in resting-state magnetoencephalography," *Clin. Neurophysiol.*, vol. 128, no. 8, pp. 1426–1437, 2017.

[4] S. Braeutigam, D. Dima, S. Frangou, and A. James, "Dissociable auditory mismatch response and connectivity patterns in adolescents with schizophrenia and adolescents with bipolar disorder with psychosis: A magnetoencephalography study," *Schizophr. Res.*, vol. 193, no. 1, pp. 313–318, 2018.

[5] P. Hansen, M. Kringelbach, and R. Salmelin, Eds., *MEG: An introduction to methods*. New York, US: Oxford University Press, 2010.

[6] R. N. Vigário, "Extraction of ocular artefacts from EEG using independent component analysis," *Electroencephalogr. Clin. Neurophysiol.*, vol. 103, no. 3, pp. 395–404, 1997.

[7] M. A. Uusitalo and R. J. Ilmoniemi, "Signal-space projection method for separating MEG or EEG into components," *Med. Biol. Eng. Comput.*, vol. 35, no. 2, pp. 135–140, 1997.

[8] T. P. Mutanen, J. Metsomaa, S. Liljander, and R. J. Ilmoniemi, "Automatic and robust noise suppression in EEG and MEG: The SOUND algorithm," *NeuroImage*, vol. 166, no. 1, pp. 135–151, 2018.

[9] M. Jas, D. A. Engemann, Y. Bekhti, F. Raimondo, and A. Gramfort, "Autoreject: Automated artifact rejection for MEG and EEG data," *NeuroImage*, vol. 159, no. 1, pp. 417–429, 2017.

[10] C. A. Joyce, I. F. Gorodnitsky, and M. Kutas, "Automatic removal of eye movement and blink artifacts from EEG data using blind component separation," *Psychophysiology*, vol. 41, no. 2, pp. 313–325, 2004.

[11] F. Rong and J. L. Contreras-Vidal, "Magnetoencephalographic artifact identification and automatic removal based on independent component analysis and categorization approaches," *J. Neurosci. Meth.*, vol. 157, no. 2, pp. 337–354, 2006.

[12] Y. Shigihara and H. Hoshi, "MEEG Automated Workflow (MEAW) System SPM toolbox," 2019. [Online]. Available: https://www.hokuto7.or.jp/hospital/lang/english-home/meaw/

[13] J. Poza, A. Bachiller, C. Gomez, M. Garcia, P. Nunez, J. Gomez-Pilar, M. A. Tola-Arribas, M. Cano, and R. Hornero, "Phase-amplitude coupling analysis of spontaneous EEG activity in Alzheimer's disease," in *Conf. Proc. IEEE Eng. Med. Biol. Soc.*, 2017, pp. 2259–2262.

[14] J. Poza, R. Hornero, D. Abásolo, A. Fernández, and M. García, "Extraction of spectral based measures from MEG background oscillations in Alzheimer's disease," *Med. Eng. Phys.*, vol. 29, no. 10, pp. 1073–1083, 2007.